

Lateral open boundary conditions for nested limited area models: A scale selective approach

P. Oddo^{a,*}, N. Pinardi^b

^a *Istituto Nazionale di Geofisica e Vulcanologia, Via Donato Creti 12, 40128 Bologna, Italy*

^b *Centro Interdipartimentale per la Ricerca in Scienze Ambientali, Università di Bologna Ravenna, Italy*

Received 8 March 2007; received in revised form 12 July 2007; accepted 21 August 2007

Available online 1 September 2007

Abstract

This paper reviews current approaches to the lateral open boundary condition problem for nested regional primitive equation ocean numerical models and proposes a new approach that considers a scale decomposition of the nesting field variables for the barotropic lateral velocity boundary conditions. The Flather [Flather, R.A., 1976. A tidal model of the north-west European continental shelf. *Memories de la Societe Royale des Sciences de Liege* 6 (10):141–164] open lateral boundary condition is derived from mass conservation considerations and we use this approach to derive a generalized lateral open boundary condition for barotropic velocities. In addition we do a scale selective decomposition of the generalized Flather obtaining new and general lateral scale dependent boundary conditions. The performance of the new lateral boundary conditions have been evaluated in two kinds of experiments: (1) idealized and (2) realistic frameworks. In the idealized framework, as well as the realistic case, the results confirms that the scale selective open boundary conditions improves the solution almost everywhere but in particular in the shallow depth parts of the model domain. In the realistic case the assessment is more difficult and it is connected also to the capability of the nesting and nested model to reproduce the dynamics contained in the observations.

© 2007 Elsevier Ltd. All rights reserved.

Keywords: Open boundary conditions; Modeling; Ocean circulation; Continuity equation; Ocean scales; Ocean processes

1. Introduction

The open boundary condition problem in numerical ocean and atmospheric modeling arises because it is not practically feasible to model the global atmosphere/ocean with a spatial resolution capable of capturing all processes of interest. Large scale circulation models have coarse horizontal resolution and are used to simulate, predict and study the large scale dynamics using an appropriate parameterization for the subgrid-scale processes. Regional (Limited Area) models are, on the contrary, used in order to resolve smaller spatial

* Corresponding author. Tel.: +39 051 4151483; fax: +39 051 4151499.
E-mail address: oddo@bo.ingv.it (P. Oddo).

and temporal scale processes. A modeling domain covering a limited area must face the problem of an adequate representation of the influence of the dynamical processes occurring outside the modeled domain on its internal dynamics.

The problem for the barotropic filtered equations has been found to be ill-posed (Bennett and Kloeden, 1978), as well as for the primitive equations (Olinger and Sundstrom, 1978). Thus the adoption of a specific open boundary condition can strongly affect the solution on the local implementation of the model. For this reason sensitivity experiments, investigating the role and the effect of different lateral open boundary conditions, play an important role in the model performance assessment. It is worth mentioning the recent work of Teman and Tribbia (2003) showing that the removal of the hydrostatic approximation in the dynamical equations reduces the ill-posedness of the problem. In our case, however, we will use primitive equations models since they are the most widespread regional ocean models used at the moment in oceanography.

As the exact solution is lacking, practical implementations of open boundary conditions in primitive equations for the oceans (Spall and Robinson, 1989) and for the atmosphere (Orlanski, 1976; Miyakoda and Rosati, 1977) have been sought. For all of these, the effectiveness of the specification adopted has to be evaluated with respect to the characteristics of the problem at hand and with regards to the spatial and temporal scales of interest. Even if the specification of prognostic variables on the open boundary is ill-posed in the pure mathematical sense, errors due to this ill-posedness may be insignificant for the flow space and time scales of interest. In this case, for any practical purpose, the boundary conditions specified may be considered viable. If, on the other hand, the boundary conditions generate or reflect waves that propagate inside the domain, or if they do not effectively transmit information into the interior, or allow information to exit, then they are not considered satisfactory (Spall and Robinson, 1989).

This paper focuses on the definition of open boundary conditions for a regional circulation model nested into a coarser model with or without different physics. A generalized Flather (1976) lateral open boundary condition is deduced for the barotropic components of the flow field. In addition, a scale selective approach is applied to the generalized Flather (1976) condition. The aim is to achieve a solution that is ‘as much as possible’ influenced only by the assumptions made on the time and space scales of the processes to be resolved in the regional versus the coarser scale model. The idea is to filter the open boundary field and define for each filtered component a specific boundary condition. We call this method a ‘scale selective approach’ to lateral boundary condition problems.

In Section 2 we provide an overview of the existing lateral boundary conditions and the derivation of the generalized Flather condition. The scale selective decomposition is described in Sections 3 and 4. This new lateral boundary condition is then implemented in a numerical model and the results for an idealized test case and a realistic simulation of the Adriatic Sea circulation are discussed in Section 5, along with the design of the sensitivity (to open boundary conditions) experiments. Section 6 offers the conclusions.

2. Lateral boundary condition formalism

A large number of open boundary conditions have been proposed in the atmospheric and oceanic dynamics in the literature. Some of them are simple schemes that nudge the prognostic variables to a reference state within a specified region in the proximity of the open boundary with an *a priori* relaxation time. Others are based on the linearization of the primitive equations of motion, thereby providing a local solution based on ‘reduced physics’. A summary of these two kinds of boundary conditions is provided below together with the description of the new solution adopted here.

2.1. Relaxation/Nudging

The relaxation/nudging scheme may be considered the simplest solution to the lateral open boundary condition problem. It consists of the addition of a Newtonian relaxation term to the model governing equations. With this technique, the model variables are driven towards a reference state originating from observations or from the results of a larger domain model. The most drastic way to do this is to impose:

$$\theta = \theta^{\text{ext}} \quad (1)$$

on the boundary, i.e. to use a Dirichlet boundary condition. This approach is often used in the context of one-way nesting (Spall and Robinson, 1989), where the values of the model variables at the lateral open boundary are obtained through a simple interpolation, in space and time, of the large scale model solutions. However, a major disadvantage of this method is that the incoming and outgoing information is totally determined by the external data irrespective of the internal solution. Therefore, due to possible inconsistencies between the external field and the interior model solution, part of the outgoing information could be reflected back into the domain.

To solve this inconsistency problem, a space dependent relaxation term is often applied to a portion of the domain in proximity to the open boundary. The return time is usually fast close to the boundary and progressively made slower proportional to the distance from the open boundary. To clarify the nomenclature we define:

– a ‘nudging term’, of the kind

$$\lambda(\theta - \theta_R) \quad (2)$$

where θ is a generic model state variable and θ_R the ‘reference’ solution. The term (2) is added to the nested domain equations and it produces the ‘relaxation’ of the solution θ to θ_R along the boundary points;

– a ‘nudging layer’ parameterized by the latitude and longitude dependency of λ , which has larger amplitude at the boundary and decreases toward the interior of the nested domain.

Another simple relaxation technique consists in artificially increasing the viscosity–diffusivity in the model interior area proximal to the lateral open boundary. This region is often defined as a ‘sponge layer’. The first obvious effect of this technique is to achieve a smoothed solution and substantially reduce the reflection of disturbances from the boundary. A sponge layer can be implemented without the imposition of external data. If used together with nudging, the sponge layer has the interesting propriety of suppressing the noise generated by the inconsistency between external and internal solutions (Palma and Matano, 1998).

2.2. Advective conditions

The advective conditions are such that the normal velocity at the boundary from the nested (regional) model is used to advect out of the domain the θ field:

$$\frac{\partial \theta}{\partial t} + V_n \frac{\partial \theta}{\partial n} = 0 \quad (3)$$

where θ indicates a generic prognostic model variable, V_n is the normal velocity at the boundary and $\frac{\partial}{\partial n}$ the normal derivative to the boundary.

Thus, external data are advected inward at inflow boundary points and the interior solution is advected outward by the regional model velocities. This simple solution has been often used (Palma and Matano, 2000; Zavatarelli and Pinardi, 2003, for example) in regional models for dynamical tracers (temperature and salinity).

2.3. Radiation conditions

The most popular open boundary conditions are derived from the Sommerfield radiation equation (1949) that provides a simple and stable extrapolation of the interior solution on the open boundary. This condition is based on the assumption that the interior solutions approaching the open boundary propagate through it in a wave-like form according to:

$$\frac{\partial \theta}{\partial t} + C \frac{\partial \theta}{\partial n} = 0 \quad (4)$$

where C is the phase speed of the waves. In special cases, it may be assumed that the wave packets approaching the boundary originate from non-dispersive gravity waves (Chapman, 1985), but a more general approach was proposed by Orlandi (1976) who estimated the phase speed inverting Eq. (4) with θ :

$$C = -\frac{\partial\theta}{\partial t} \left(\frac{\partial\theta}{\partial n} \right)^{-1}. \quad (5)$$

The numerical stability requirements are that $0 \leq C \leq \Delta x / \Delta t$, where Δx and Δt are the spatial and temporal steps, respectively. If C exceeds the stability value for (5) the maximum value of C is imposed on the boundary point. Conversely, for low values of C , its value can be prescribed using external information or simply persisting the previous time-step value. A 2D Sommerfeld radiation has been proposed by Raymond and Kuo (1984). The new derivation of the radiation condition takes into account both the normal and tangential component of the wave phase speed, giving:

$$\frac{\partial\theta}{\partial t} + C_x \frac{\partial\theta}{\partial x} + C_y \frac{\partial\theta}{\partial y} = 0 \quad (6)$$

where the subscripts x and y are, respectively, the normal and the tangential direction to the boundary in local Cartesian coordinates. We call the boundary condition (6) the ‘oblique radiation’ condition.

The two phase speeds can be calculated from the surrounding interior grid point:

$$C_x = -\frac{\partial\theta}{\partial t} \frac{\partial\theta/\partial x}{(\partial\theta/\partial x)^2 + (\partial\theta/\partial y)^2} \quad (7)$$

$$C_y = -\frac{\partial\theta}{\partial t} \frac{\partial\theta/\partial y}{(\partial\theta/\partial x)^2 + (\partial\theta/\partial y)^2}. \quad (8)$$

It has to be pointed out that the derivation of the two phase speeds makes sense only in a discrete form (Raymond and Kuo, 1984). The advantage resulting from this 2D calculation is the increased accuracy in the computation of the normal component of the phase speed, particularly when the direction of propagation has a significant tangential component.

The idea proposed by Orlandi (1976) also provides the basis for other open boundary conditions accounting for a selective treatment of inward and outward fluxes. Miyakoda and Rosati (1977) suggested prescribing the external information at inflow points and using the wave equation in order to obtain the open boundary solution at outflow (this solution in the literature is called ‘‘Modified Orlandi Radiation’’). The problem is that an inconsistency could be generated at the boundary points where the flow field switches in time between the two regimes. A possible solution to this problem has been proposed by Marchesiello et al. (2001), by simply adding a nudging term to (6):

$$\frac{\partial\theta}{\partial t} + C_x \frac{\partial\theta}{\partial x} + C_y \frac{\partial\theta}{\partial y} = -\frac{1}{\tau} (\theta - \theta^{\text{ext}}) \quad (9)$$

where θ^{ext} represents the external data or solution and τ is the time scale for the nudging term.

The authors suggest and test the idea of using different time scales for the nudging term depending on the inflow–outflow regime. According to the authors the advantage obtained having a small relaxation also during the outflow regimes is to prevent possible model drift that can cause large differences between the regional model solution and the external or coarser model solution. An interesting variation of this method has been used in Lermusiaux (2007) where the relaxation time depends on depth. According to the author, this depth dependent formulation allows a better radiation of surface structures and waves.

2.4. Mass conservation equation: the Flather condition for barotropic velocities

An interesting and useful solution for the open boundary conditions was proposed by Flather (1976). This condition can be classified as a special case of the radiation condition. Here we discuss this solution separately from the other radiation conditions in order to emphasize its derivation and physical meaning.

The Flather (1976) condition originates from an attempt to simulate the principal semi-diurnal tide on the north-west European continental shelf using a limited-area 2D numerical ocean model. The influence of

different open boundary conditions on the internal solution was investigated. The most satisfactory results were obtained by prescribing a relationship between elevation and currents at the open boundary arising from a combination of the continuity equation with a radiation condition. Here we derive the boundary condition equation used by Flather (1976). Other derivations have been proposed in the recent literature (Blayo and Debret, 2005) but we believe our method highlights the physical interpretation of the derivation and it generalizes the Flather condition making it applicable to a large number of different conditions.

Let us take the incompressible continuity equation

$$\nabla \cdot \vec{u} = 0$$

where $\vec{u} = (u, v, w)$ is the total velocity field. Integrating between the surface, $\eta(x, y, t)$ and the bathymetry, located at $-H(x, y)$, we obtain:

$$\frac{\partial \eta}{\partial t} + \nabla \cdot [(H + \eta) \vec{V}_{BT}] = 0 \quad (10)$$

where now \vec{V}_{BT} is the horizontal barotropic flow field, defined by:

$$\vec{V}_{BT} = \frac{1}{H + \eta} \int_{-H}^{\eta} (u, v) dz. \quad (11)$$

In Table 1 we now define the coarse model variables and the regional or fine resolution model state variables.

The hypothesis here is that each model separately conserves mass as written in (10). Thus it will be possible to equate the two mass conservation equations obtaining:

$$\nabla \cdot [(H_c + \eta_c) \vec{V}_{BTc}] + \frac{\partial \eta_c}{\partial t} = \nabla \cdot [(H_f + \eta_f) \vec{V}_{BTf}] + \frac{\partial \eta_f}{\partial t}. \quad (12)$$

Assuming now that the surface elevation tendency is given by a radiation equation like (6) we have:

$$\frac{\partial \eta}{\partial t} = -\nabla \cdot (\vec{C}\eta). \quad (13)$$

Inserting (13) into (12) and assuming that both the coarse (nesting) and fine (nested) resolution models have the same wave phase speed, we obtain the relationship for the normal barotropic velocity component, V_{BT}^n as follows:

$$V_{BTf}^n = \frac{H_c + \eta_c}{H_f + \eta_f} V_{BTc}^n - \frac{C^n}{H_f + \eta_f} (\eta_c - \eta_f) \quad (14)$$

where C^n is the normal component of the wave phase speed: we call (14) a generalized Flather's boundary condition.

We now suppose that the normal component of the phase speed is the linearized free gravity wave speed $C^n = \sqrt{gH}$, that $H_c = H_f = H$ and $|\eta| \ll H$ so that (14) becomes:

$$V_{BTf}^n = V_{BTc}^n - \frac{\sqrt{gH}}{H} (\eta_c - \eta_f). \quad (15)$$

Eq. (15) is the well known Flather (1976) lateral boundary condition equation.

Table 1

State variables of the coarse and fine resolution models used to derive the Flather equation. The scale decomposition is also shown for the fine resolution model

Model	Barotropic velocity	Surface elevation
Coarse resolution	\vec{V}_{BTc}	η_c
Fine resolution (Total component)	\vec{V}_{BTf}	η_f
Fine resolution (Global component)	\vec{V}'_{BTf}	η'_f
Fine resolution (Regional component)	\vec{V}''_{BTf}	η''_f

3. The scale selective lateral boundary condition

Oceanic physical processes, forced by surface stresses, display structures as a result of nonlinear interactions between the scales composing the motion. No model can represent the entire spectrum of events from molecular processes to climatic bifurcations, therefore an essential characteristic of a model is its spectral window. The choice of a spectral window defines a model and, obviously, the scales at which the state variables are resolved (Nihoul and Djenidi, 1998). As discussed in the introduction, the use of limited area models derives from the necessity of resolving smaller scale processes that are not adequately resolved in the coarser model or, in other words, it derives from the necessity to move from one spectral window to another. This necessarily implies an inconsistency between the regional model solution and the external, coarser model data.

For a one-way nesting the inconsistency is amplified if the external fields are averaged in time and supplied with a given frequency that is defined *a priori*. In a time averaged field all the processes with a frequency higher than the time window used for computing the mean are filtered out (the characteristic model spectral window is furthermore redefined) and this should be considered when nesting models within these prescribed fields. Furthermore, the mismatch between interior solution and externally imposed boundary conditions may generate numerical instability and/or the insurgence of numerical noise in the interior area close to the boundary.

In order to try to avoid some of these problems, we suggest a new approach based on the splitting of the nested model internal solution into two different parts: the first containing the physics represented in the external and/or coarser model; the second containing the processes characteristics of the nested model.

3.1. The scale decomposition

In view of the scale selective approach of this paper, we apply a decomposition that separates a nested model fields as follows:

$$\theta_f = \theta'_f + \theta''_f.$$

Where θ'_f is the portion of the solution belonging to the overlapping spectral window between nesting and nested models, and θ''_f is a component specific of the nested model spectral window. Hereafter we will refer to θ'_f as the “global” field and to θ''_f as the “regional” field, following the nomenclature of Table 1. We can speculate now on what to use for the two components: one choice is to impose θ'_f to be equal to the nesting model fields, which we call θ^{ext} using Eq. (1). This means that θ''_f can be obtained as the difference between nesting and nested model state variables ($\theta''_f = \theta_f - \theta^{\text{ext}}$). If we use then any radiation condition (Eq. (4) or Eq. (6)) for θ''_f we obtain the lateral open boundary conditions of Perkins et al. (1997). The latter shows that the lateral boundary conditions applied to θ''_f give better results if compared to standard radiation applied to the full regional field (Perkins and Smedstad, 1998; Perkins et al., 1997). In this paper we revisit the results by Perkins et al. (1997) generalizing it to a scale selective approach applied to the barotropic velocity lateral boundary conditions.

3.2. A scale selective method for the barotropic mode lateral boundary condition

We proceed now applying the scale selective approach to the derivation of the generalized Flather open boundary condition of Section 2.4. We use the scale decomposition for the free surface field as:

$$\eta_f(x, y, t) = \eta'_f(x, y, t) + \eta''_f(x, y, t) \quad (16)$$

and for the barotropic velocity field as

$$\vec{V}_{\text{BT}f}(x, y, t) = \vec{V}'_{\text{BT}f}(x, y, t) + \vec{V}''_{\text{BT}f}(x, y, t). \quad (17)$$

Here again η'_f and $\vec{V}'_{\text{BT}f}$ are the global components, and η''_f and $\vec{V}''_{\text{BT}f}$ indicate the part resolved only by the fine resolution model (see Table 1). Rewriting the *r.h.s* of Eq. (12) taking into account the decomposition we obtain:

$$\nabla \cdot [(H_c + \eta_c)(\vec{V}_{BTc})] + \frac{\partial \eta_c}{\partial t} = \nabla \cdot [(H_f + \eta'_f + \eta''_f)(\vec{V}'_{BTf} + \vec{V}''_{BTf})] + \frac{\partial \eta'_f}{\partial t} + \frac{\partial \eta''_f}{\partial t}. \quad (18)$$

We now solve (18) by equating the *l.h.s.* to the part of the *r.h.s.* which contains only the global components of the nested fields, while the regional parts are imposed to be equal to zero separately. Thus, for the global component, we obtain:

$$\nabla \cdot [(H_c + \eta_c)(\vec{V}_{BTc})] + \frac{\partial \eta_c}{\partial t} = \nabla \cdot [(H_f + \eta'_f)\vec{V}'_{BTf}] + \frac{\partial \eta'_f}{\partial t} \quad (19)$$

and for the regional component:

$$\nabla \cdot [(H_f + \eta_f)\vec{V}''_{BTf} + \eta''_f\vec{V}'_{BTf}] + \frac{\partial \eta''_f}{\partial t} = 0 \quad (20)$$

Following the same procedure as before, we assume a radiation condition for the tendencies:

$$\frac{\partial \eta_c}{\partial t} = -\nabla \cdot (\vec{C}'\eta_c) \quad (21)$$

$$\frac{\partial \eta'_f}{\partial t} = -\nabla \cdot (\vec{C}'\eta'_f) \quad (22)$$

where \vec{C}' is the phase speed for the global field that is considered again to be equal for the nesting and nested model fields. The phase speed can be obtained by assuming a gravity wave dispersion relationship or, as suggested by [Orlanski \(1976\)](#), solving the wave equation using the interior values. Substituting (21), (22) in (19) we obtain:

$$\nabla \cdot [(H_c + \eta_c)(\vec{V}_{BTc})] - \nabla \cdot (\vec{C}'\eta_c) = \nabla \cdot [(H_f + \eta'_f)\vec{V}'_{BTf}] - \nabla \cdot (\vec{C}'\eta'_f).$$

Solving for the normal component of \vec{V}'_{BTf} we obtain the solution for the global part of the nested model barotropic velocity:

$$V'_{BTf} = \frac{H_c + \eta_c}{H_f + \eta'_f} V_{BTc} - \frac{C'^n}{H_f + \eta'_f} (\eta_c - \eta'_f). \quad (23)$$

This is the generalized [Flather \(1976\)](#) lateral boundary condition written in (14) but now alone for the global component of the nested fields. Assuming $H_c = H_f = H$ and $|\eta'_f|, |\eta_c| \ll H$ we obtain:

$$V'_{BTf} = V_{BTc} + \frac{C'^n}{H} (\eta'_f - \eta_c). \quad (24)$$

This is the well known Flather equation with the one difference that the phase speed is not fixed *a priori* and only the global component of the nested model sea level is considered. Once the open boundary condition for the global component of the nested model is obtained, we can re-write (20) for the regional component:

$$\nabla \cdot [(H_f + \eta_f)\vec{V}''_{BTf} + \eta''_f\vec{V}'_{BTf}] - \nabla \cdot (\vec{C}''\eta''_f) = 0 \quad (25)$$

where we assumed again that wave motion is dominant in order to explain the tendency of the regional component of the surface elevation, i.e.:

$$\frac{\partial \eta''_f}{\partial t} = -\nabla \cdot (\vec{C}''\eta''_f).$$

Solving for V''_{BTf} we obtain the solution for the regional component of the fine resolution model barotropic velocity normal to the boundary:

$$V''_{BTf} = (C''^n - V_{BTc}) \frac{\eta''_f}{H_f + \eta_f} = \frac{\eta''_f}{H} \left(C''^n - V_{BTc} - \frac{C'^n}{H} (\eta'_f - \eta_c) \right) \quad (26)$$

where $H_f = H$ and $|\eta_f| \ll H$ has been used together with (24). In the case of (26) the value for the regional component of the normal barotropic velocity at the boundary depends directly on η''_f . In the Flather

condition (15) this problem is mitigated by the last term in the equation that is only the difference between the two surface elevations. On the contrary, the physical meaning of the term $\frac{\eta_f'}{H}$ present in (26) is not clear; it is evident however that the contribution of (26) will be important in shallow topography regions where H is small.

Our new set of “scaled” open boundary conditions for the normal barotropic velocities are given by (24) and (26) provided one subdivides the fine resolution model fields into global and regional components.

4. A special case: nesting a free surface in a rigid lid model

A reasonable approximation of the large scale ocean dynamics is the rigid lid approximation. This approximation filters out the fast barotropic gravity waves by setting the time variation of the free surface elevation equal to zero. Thus our derivation of the Flather equation has to be re-written for this special case. We proceed first deriving the barotropic lateral boundary condition for this special case, and then use the new proposed scale selective boundary condition derivation. For a free surface model nested within a rigid lid coarser model (12) becomes:

$$\nabla \cdot (H_c \vec{V}_{BTc}) = \nabla \cdot [(H_f + \eta_f) \vec{V}_{BTf}] + \frac{\partial \eta_f}{\partial t}. \quad (27)$$

Note that the *l.h.s.* of (27) has no η_c in the continuity equation. If also zero tendency is assumed for η_f in the *r.h.s.* of (27), the velocity component normal to the open boundary is:

$$V_{BTf}^n = \frac{H_c}{H_f + \eta_f} V_{BTc}^n. \quad (28a)$$

Eq. (28a) has been used in Zavatarelli et al. (2002) and Zavatarelli and Pinardi (2003) for a free surface nested into a rigid lid model, similar to the one used in this paper.

Solving now the complete Eq. (27), using (13) for the linear gravity wave speed of the free surface tendency, taking $H_c = H_f = H$ and assuming $|\eta_f| \ll H$ we obtain:

$$V_{BTf}^n = V_{BTc}^n + \frac{\sqrt{gH}}{H} \eta_f'. \quad (28b)$$

Eqs. (28a) and (28b) are the Flather (1976) classical boundary conditions for the nesting of a free surface with a rigid lid model.

Considering now the scale decomposition approach described in Section 3, the equivalent of (23) for the global component is:

$$V_{BTf}^n = \frac{H_c}{H_f + \eta_f'} V_{BTc}^n + \frac{C^n}{H_f + \eta_f'} \eta_f'. \quad (29)$$

while (26) for the regional component remains the same. If $H_c = H_f = H$ and $|\eta_f'| \ll H$ (29) becomes:

$$V_{BTf}^n = V_{BTc}^n + \frac{C^n}{H} \eta_f'. \quad (30)$$

Thus for the rigid lid coarse resolution models that use nested free surface models, the scale selective boundary conditions are given by (29) and (26).

5. Sensitivity experiments to lateral boundary conditions

The performances of the scale selective approach applied to lateral boundary conditions were tested in a series of numerical simulations that included idealized and realistic test cases. In the idealized case, the Flather (1976) boundary condition (15) is applied and evaluated against the corresponding scale selective Eqs. (23) and (26). In the realistic framework experiment, the scale selective approach has been evaluated in the case of a free surface model nested into a rigid lid model (Eqs. (29) and (26)).

5.1. Idealized test case

In this section, the sensitivity of the model results to the “scale selective” approach is investigated by means of a direct comparison between simulations in an idealized ocean with and without the scaled lateral boundary conditions. Using the Princeton Ocean Model (POM, [Blumberg and Mellor, 1987](#)) two numerical nested simulations have been carried out progressively increasing the complexity of the simulated system. The general result is that the differences between lateral boundary conditions are amplified increasing the complexity of the simulated flow field.

The simulations have been done in a ‘twin experiment’ set-up: two reference ocean states have been obtained performing two model simulations on an extended domain with a regular horizontal grid 310 km long and 320 km wide (with 4 km horizontal resolution) and 21 vertical sigma layers. For both of them the model bathymetry reproduces a zonal sea channel as illustrated in [Fig. 1a](#). In the first experiment the model has been initialized with horizontally homogeneous density field, while in the second experiment an initial horizontal density gradient has been introduced (together with balanced geostrophic currents) as illustrated in [Fig. 1c](#). In both cases the model density is a function of depth ([Fig. 1b](#)). We consider experiment 1 a simplified physical model with respect to experiment 2. At the surface, both models are forced with an analytical wind stress simulating the passage of an atmospheric cyclonic structure similar to [Palma and Matano \(1998\)](#) study case. Several storm configurations have been evaluated all producing similar results; in the present experiments the storm is characterized by a radius of 50 km, a maximum wind stress intensity of 10 dyne cm^{-2} , and a storm centre velocity of 0.3 m s^{-1} . The model has been integrated for 10 days using (4) on the Western and Eastern sides of the channel. The results of these two simulations have been considered as the reference ocean state.

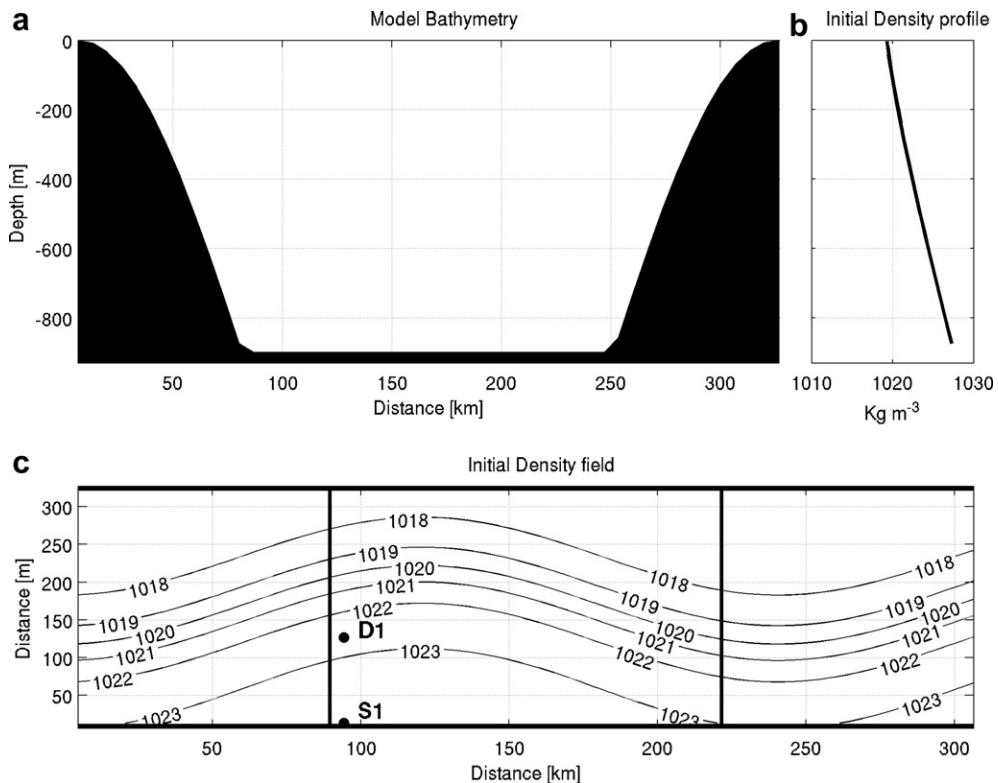


Fig. 1. Idealized model test case configuration. (a) latitudinal model bathymetry section. (b) Initial density vertical profile (units are kg m^{-3}). (c) Contours of the initial horizontal density pattern for the second experiment. The nested model domain is shown by the two vertical lines at the centre of the channel. Location S1 and D1 are indicated in (c).

The boundary condition experiments have been performed implementing a model nested on a sub-region of the reference experiment domain (same latitudinal extension but reduced longitudinal dimension see Fig. 1c). The simulations have been initialized using a “restart” generated from the reference experiments on day 1, which also supplied boundary condition data in terms of daily means of all the requested model variables. The nesting and nested models have then the same resolution but the boundary condition fields are averaged in time, filtering high frequencies and small scale features from the diagnosed fields in order to simulate a coarser resolution nesting model output. During the simulations the lateral boundary conditions data have been linearly interpolated to the model time-step.

Two different models, nested in the two reference states, have been implemented on the basis of the normal barotropic velocity lateral boundary condition: Model-1 uses the standard Flather (1976) formulation (15), Model-2 makes use of the corresponding scaled Eqs. (23) and (26). In both models the zero gradient boundary condition for the surface elevation is used, (1) has been used for the barotropic tangential velocity and the “Modified Orlanski radiation” (4) has been used for tracers.

In Model-2 the surface elevation global component (η' in Eq. (16)) is computed performing at each model time-step a 24 h running mean centred 12 h back in the past. The normal phase speeds of the global (C^n in Eq. (23)) and regional (C'^n in Eq. (26)) components have been obtained using Orlanski formulation (Eq. (5)). For both phase speeds we set the limit of C^n and C'^n to the linear gravity wave value (\sqrt{gH}).

Fig. 2 shows snapshots of sea surface elevation contours after 4.5 days for the reference experiment 1 and 2 and Model-1 and Model-2 experiments. In the first experiment (horizontally homogeneous density field) the results are similar to those discussed by Palma and Matano (1998) and both boundary condition configurations perform similar to the reference experiment. Introducing a horizontal density gradient in the reference experiment 2, amplifies the differences between Model-1 and Model-2. The surface elevation field in the extended domain (Fig. 2) is characterized by a south–north positive gradient and a cyclonic structure generated directly by the wind stress is elongated across the domain. Both Model-1 and Model-2 failed to correctly represent the coastal waves travelling along the Northern side of the channel but Model-1 more than Model-2 and the intensity of the cyclonic circulation is better represented in Model-2.

A quantitative evaluation of the differences between Model-1 and Model-2 has been carried out using horizontal and/or temporal mean estimates of root-mean-square-error (RMSE) and pattern correlation

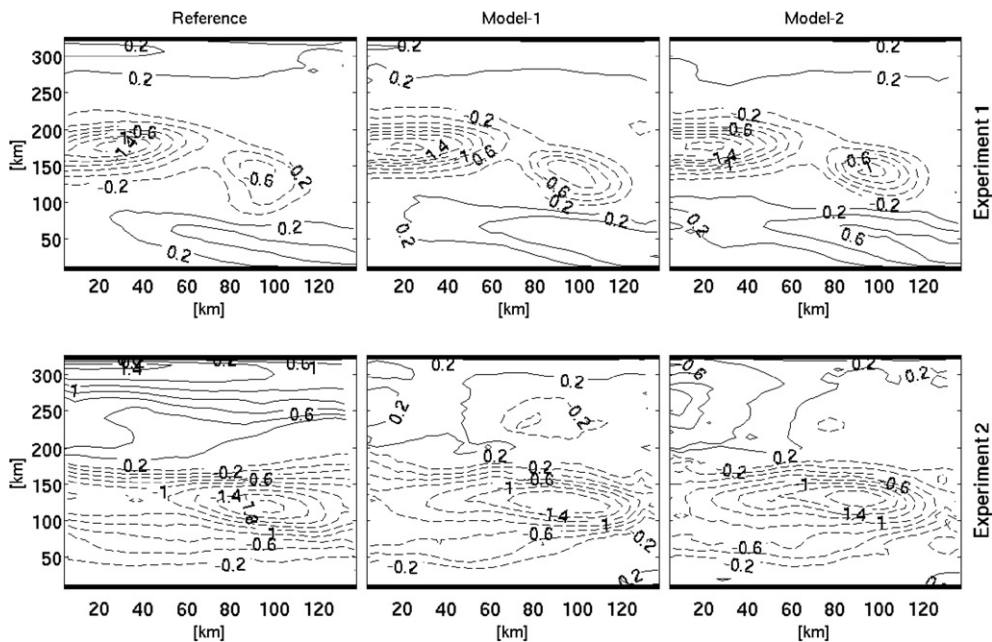


Fig. 2. Surface elevation contours snapshot at day 4.5 after the start. The top panels show results for the first experiment. The lower panels show results of the second experiments. Contour interval is 0.2 m.

coefficient (PCC) defined according Lermusiaux (2007) and computed by taking differences between the reference and Models-1–2 solutions.

In Fig. 3 the time series of surface elevation PCC (Fig. 3a) and RMSE (Fig. 3b) averaged over the whole model domain are shown. In the first experiment PCC and RMSE give opposite results. After 5 days Model-1 and Model-2 results start to differ, the scale selective lateral boundary condition improves the PCC but the RMSE gets worse indicating that a bias is introduced. In experiment 2, the PCC and RMSE give coherent results having high PCC values associated with low estimated RMSE; in average the scale selective approach improves model results of about 5% compared to the standard formulation.

The different behavior of the lateral open boundary condition imposition is more evident in Fig. 4 where a distinction is made between point S1 and D1 (see Fig. 1) time series of zonal barotropic velocities. We observe that the largest differences between Model-1 and Model-2 are confined in the shallow areas. As already pointed out in Section 3, (26) is important in shallow water regions because of the presence of the $\frac{u}{H}$ factor which is large when H is small. Imposing daily averaged fields as boundary values together with a standard Flather (1976) condition (15) does not allow the high frequency components of the solution (regional component) to be maintained in the proximity of the lateral boundaries even if the nested model produces them.

On the other hand, the scale selective approach, treating separately global and regional components, improves the simulated shelf waves, partly removing the bias. In the deep ocean areas, Model-1 and Model-2 are similar because (26) gives $V''_{BTf} \approx 0$ and (15) and (23) become almost identical. In this case, both Flather (1976) and the scale selective lateral boundary conditions act as a smoother for the high frequencies, as clearly shown in Fig. 4. Therefore with the increasing of water depth the high frequencies are filtered out regardless of the nesting method.

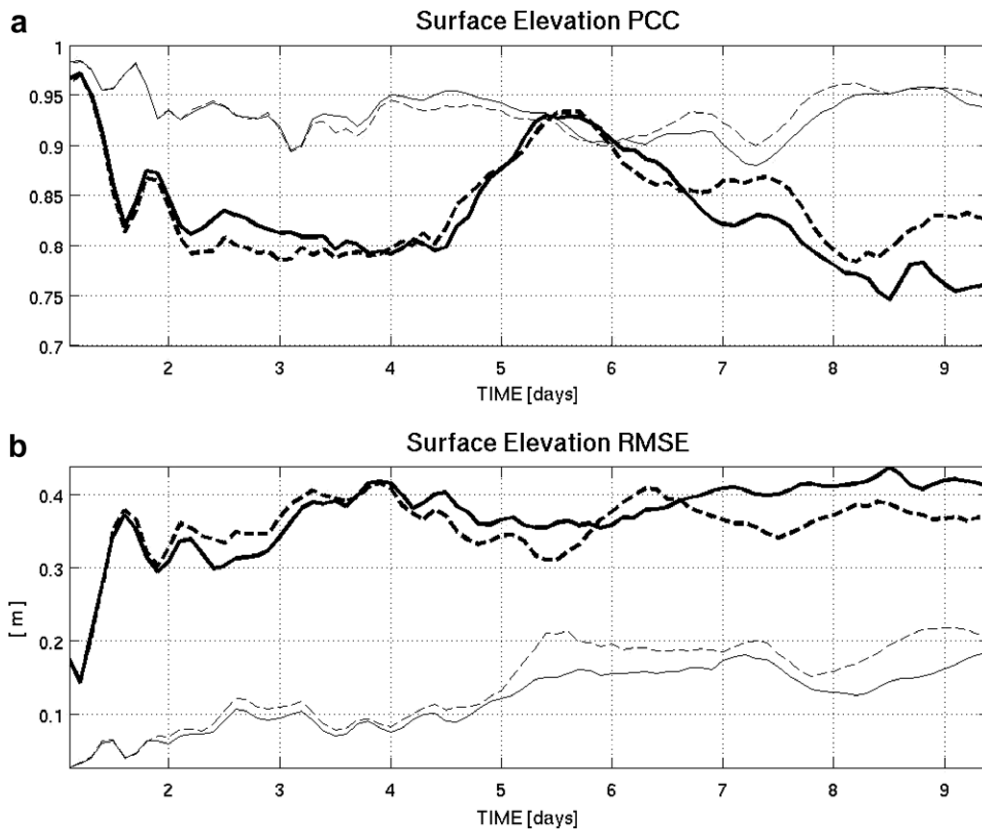


Fig. 3. Time series of: (a) PCC; (b) RMS differences in meters. Solid lines indicate Model-1 results, dashed lines indicate Model-2 results (thin for the first experiment, bold for the second).

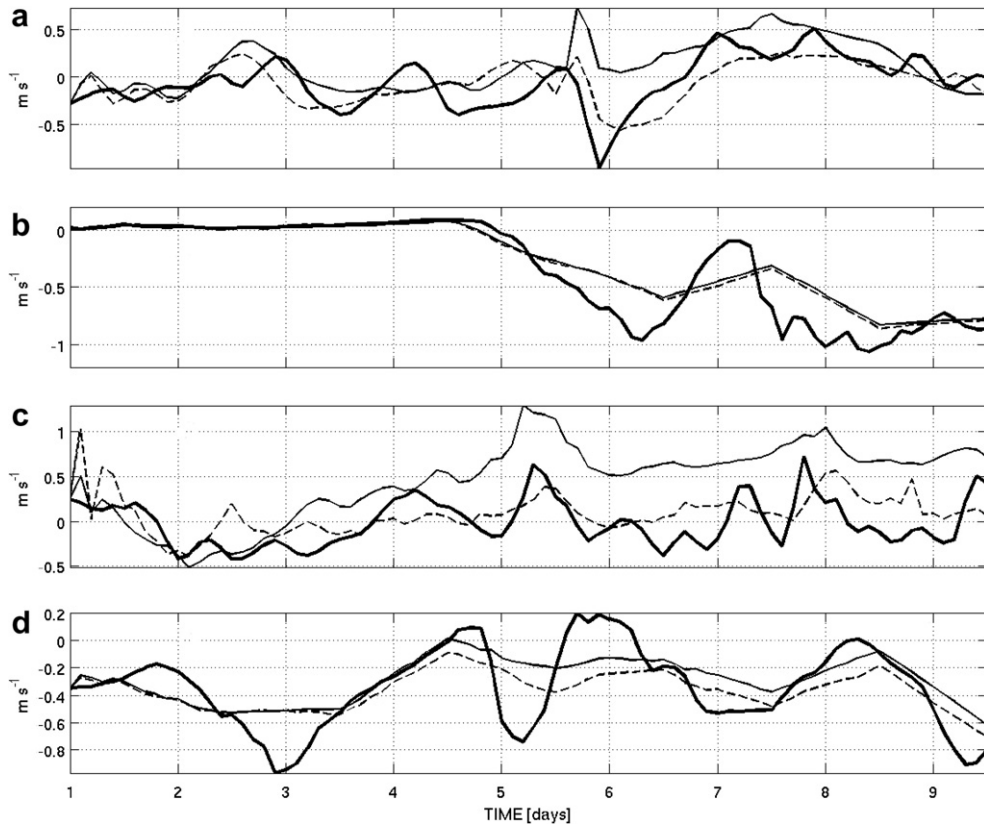


Fig. 4. Time series of the zonal barotropic velocity for the reference simulation (solid bold lines), Model-1 (solid lines) and Model-2 (thin dashed lines). Panels A and B indicate results of the first experiment for a shallow water location (A) and deep ocean (B). Panels C and D show results for the second experiment (S1 shallow water point; D1 deep ocean point).

5.2. Realistic test case

In this section we show simulations carried out to illustrate the sensitivity of the solution of a realistic regional model to different lateral open boundary conditions. The region of interest is the Adriatic Sea; the nesting model is a rigid lid Mediterranean general circulation model while the nested model is free surface. The modeling system used in this study has been implemented in the framework of the ADRIatic sea integrated COastal areaS and river basin Management system Pilot Project (ADRICOSM) and it is currently operational producing weekly forecast for the Adriatic Sea (Oddo et al., 2006). The performance of the new scaled lateral boundary conditions (26) and (29) will be tested by comparing with in situ data.

5.2.1. Numerical model set up

The numerical model used to test the different boundary conditions performance is based on the Princeton ocean model (POM, Blumberg and Mellor, 1987) and it has been described in detail by Zavatarelli and Pinardi (2003) and Oddo et al. (2005).

Fig. 5 illustrates the modeling domain. At the open boundary the sub-regional model with approximately 5 km horizontal resolution is one-way nested with the operational $1/8^\circ$ resolution model of the entire Mediterranean (Demirov and Pinardi, 2002; Pinardi et al., 2003) which provides daily averaged temperature, salinity and velocity fields used for open boundary specifications. The two models resolve different processes having different horizontal resolutions but also different physics (the major differences between the models are listed in Table 2). Both models interactively compute the surface fluxes using the atmospheric fields provided by ECMWF (European Centre for Medium range Weather Forecast) analyses (Pinardi et al., 2003).

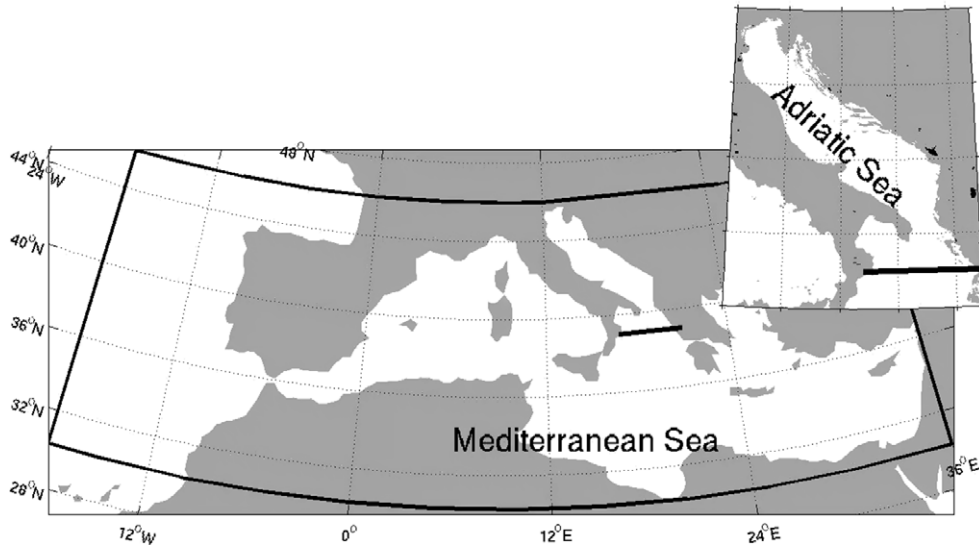


Fig. 5. Schematic representation of the modeling domains. The coarse resolution model ($1/8^\circ$ horizontal resolution) covers the entire Mediterranean Sea and provides lateral open boundary data to the fine resolution model ($1/22^\circ$ horizontal resolution) covering the Adriatic Sea (zoom).

Table 2

Summary of some of the major regional (POM) and global (MOM) models differences

	Regional	Global
Horizontal resolution	$1/22^\circ$	$1/8^\circ$
Vertical resolution	21σ	31ζ
Ocean Surface	Explicit free surface	Rigid lid
Horizontal diffusion coefficient	Smagorinsky (1993)	Constant and bi-harmonic
Vertical diffusion coefficient	Mellor and Yamada (1982)	Constant

In all the experiments described in the next section, a nudging and a sponge layers have been implemented for dynamical tracers as follows:

$$\frac{\partial \gamma}{\partial t} = -\vec{v} \cdot \vec{\nabla} \gamma + \lambda \vec{\nabla}_h \cdot (K_h \vec{\nabla}_h \gamma) + \frac{\partial}{\partial z} \left(K_v \frac{\partial \gamma}{\partial z} \right) - \frac{1}{\tau} (\gamma - \gamma_C) \quad (31)$$

where γ indicates either temperature or salinity, γ_C is the coarse resolution field, K_h the horizontal and K_v vertical diffusivities, $\vec{\nabla}$ the 3D gradient operator, $\vec{\nabla}_h$ the horizontal gradient operator. τ varies linearly from 30 days at the boundary to 10 years at a distance from the open boundary of approximately 90 km. Here λ is the non dimensional sponge layer factor that depends on latitude and longitude. The sponge layer has been used in an area extending approximately 50 km north of the open boundary where λ linearly increases from 1 to approximately a factor of 2 at the boundary.

The simulations span the period from January 1999 to the end of 2001. As initial conditions we used the results of a climatological simulation (Zavatarelli and Pinardi, 2003). The simulation for the year 1999 has been performed using a single set of boundary conditions. Then year 2000 is considered as a spin up period for the different boundary condition sets and the results of the simulations are compared for year 2001.

5.2.2. Design of the numerical experiments

Several set of boundary conditions have been implemented but only those that give stable solutions (Table 3) are discussed in the following sections. In all the experiments we used a zero gradient boundary condition for the free surface elevation.

Table 3

The boundary conditions used in the three experiments. U and V indicate the barotropic velocity, u and v the total velocity and T and S indicate Temperature and Salinity, respectively

	Exp1R	Exp2R	Exp3R
U, V	Imposed	2D radiation + nudging	Scale decomposition
u, v	Imposed	2D radiation + nudging	Imposed
T,S	Advection scheme	2D radiation + nudging	Advection scheme
Nudging layer	90 km with τ (Eq. (31)) linearly varying from 10 years to 1 month		
Sponge layer	50 km with λ (Eq. (31)) linearly varying from 1 to 2.4		

The first experiment (Exp1R) was carried out by imposing barotropic and total velocities from the coarse resolution model (see Eq. (1)), while a simple advection scheme (Eq. (3)) has been used for tracers. The second experiment (Exp2R) was carried out using for all the prognostic variables the 2D version of the radiation condition as suggested by Marchesiello et al. (2001) (our Eqs. (6)–(8)). The third experiment (Exp3R) was carried out using the same boundary conditions of Exp1R but applying the scaled version of the generalized Flather open boundary condition (26) and (29).

In order to obtain the global and regional fields decomposition for the free surface elevation, the global component of the nested free surface field is set equal to the η_r derived from the sea surface pressure formulation of rigid lid models (Pinardi et al., 1995). Thus the free surface decomposition (16) is

$$\eta_f = \eta_r + \eta_f'' \quad (32)$$

Eq. (29) has been used in the simplified form (30). Eq. (26) has then been used to solve the regional component by imposing zero phase velocity for the regional part of the surface elevation so that:

$$\vec{V}_{BTf}'' = -\vec{V}_{BTf}^m \frac{\eta_f''}{H + \eta_f} \quad (33)$$

For the barotropic velocities fields an interpolation constraint has been used (Pinardi et al., 2003). This constraint allows the total transport to be maintained after interpolation from the coarse to the fine resolution grid. The method consists of calculating the total volume transport through the open boundary and uniformly adjusting the barotropic inflow–outflow at the open boundary, in order to exactly preserve the total volume.

5.2.3. Results and discussion

In this section we present the results obtained by using the different boundary conditions in the realistic experiments. The difference between the experiments has been studied by means of the root mean square (RMS) difference between each model results and observations. Two different sets of observations have been used to compute the RMS error: XBT data and CTD data from NATO-NURC ADRIA01 cruise.

Four different XBT cruises have been performed in year 2001: 4–6 April; 20–23 Jun; 30–31 October and 2–3 December. In Fig. 6 the temperature RMS error vertical profiles of the Exp1R are shown together with the corresponding relative performance (RP) index for the other two experiments. The RP has been defined as the ratio between RMS error of Exp2R or Exp3R with respect to Exp1R, therefore RP values < 1 indicate an improvement in numerical simulation while RP value > 1 show a deterioration. In April Exp1R and Exp2R have similar performance (the Exp2R RP is close to 1 all along the water column) while Exp3R boundary conditions set-up has reduced RMS error especially between 100 and 200 m, with an averaged improvement of about 14%. In June all the experiments have similar behavior in terms of RMS error except in the upper layer. Moreover, considering RMS error vertical averages, the 2D radiation condition is characterized by larger values (1% worst than Exp1R) while the scale decomposition approach always results in small improvements (5% better than Exp1R). October is the only month where 2D radiation performs better than the scale decomposition approach (Exp2R RP is 10% while Exp3R RP is close to 4%), the two RP curves have similar shape but below 100 m Exp2R has a constant and smaller RMS values. In December the model solution seem to be strongly affected by the boundary condition choices and a large improvement derives from the scale

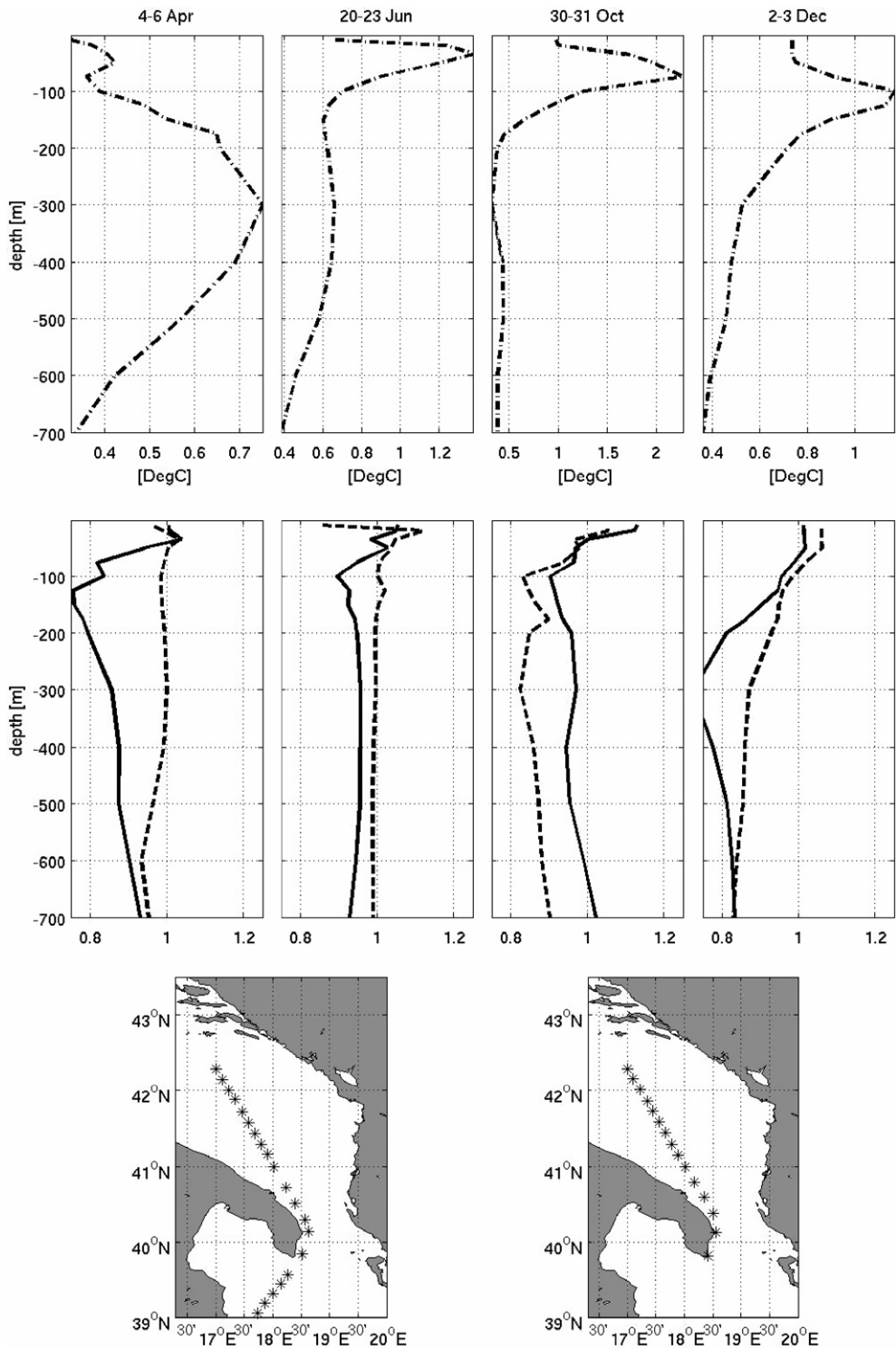


Fig. 6. Vertical profiles of Temperature RMS error for the different XBT cruises tracks (April, June, October and December). The first row shows the vertical profiles of RMS error for the reference experiment (Exp1R). In the second row the Relative Performance indices (RP) of Exp2R (dashed line) and Exp3R (solid line) are shown (RP is defined as the ratio between Exp2R or Exp3R and Exp1R RMS values). The lower plots show the position of the XBT tracks for the April–June and October–December cruises, respectively.

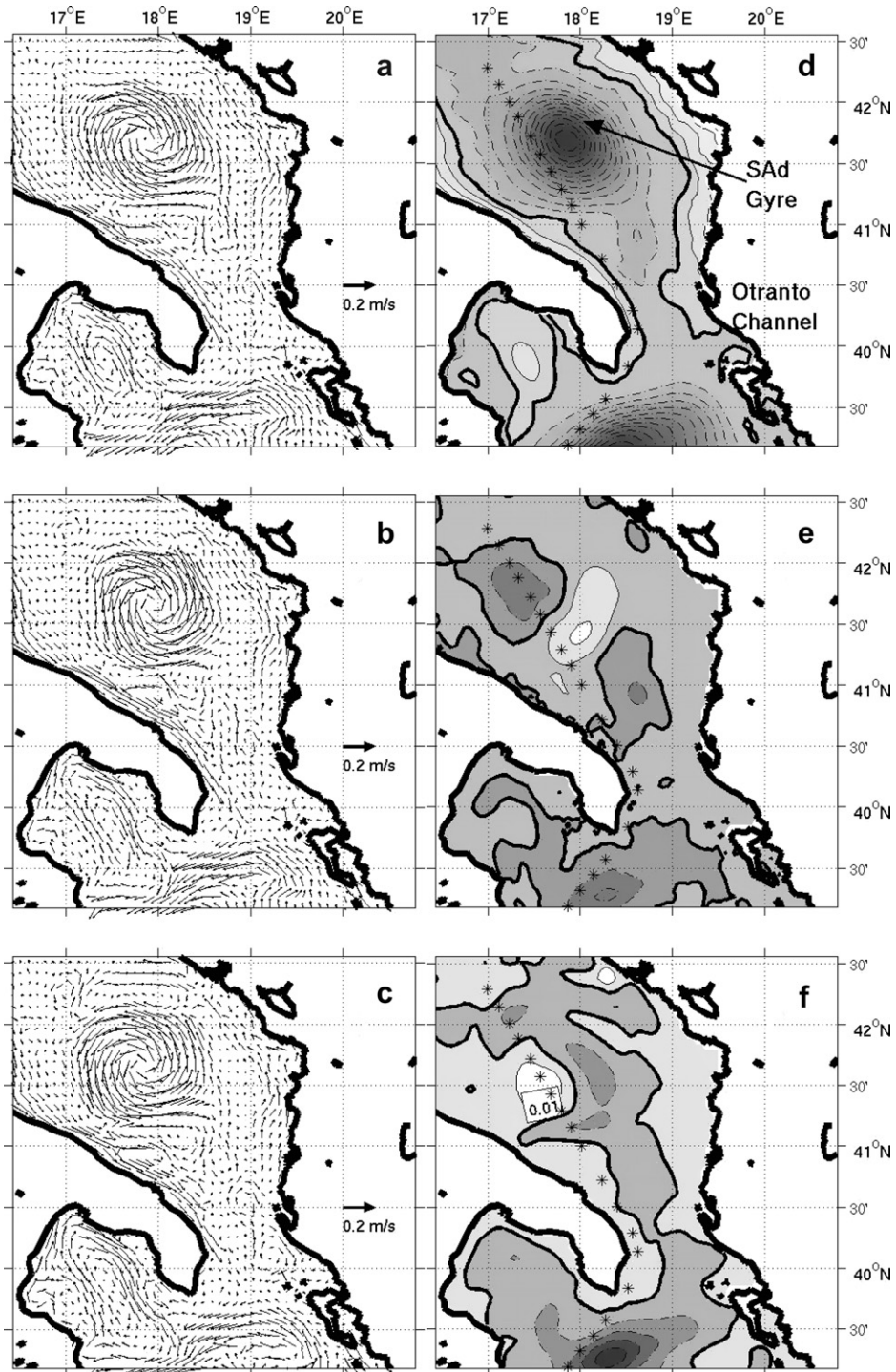


Fig. 7. Horizontal maps of barotropic velocity and surface elevation for the three experiments. Panels A B and C indicate barotropic velocity for the Exp1R Exp2R and Exp3R, respectively. In panels D the surface elevation field for Exp1R is shown. In panels E and F only the surface elevation differences between Exp2-Exp1 (E) and Exp3-Exp1 (F) are shown. The fields have been obtained averaging the model results from 4 to 6 April C.I in the surface elevation plots is 1 cm. Dashed lines indicate negative values and the thick black line is indicating the null value.

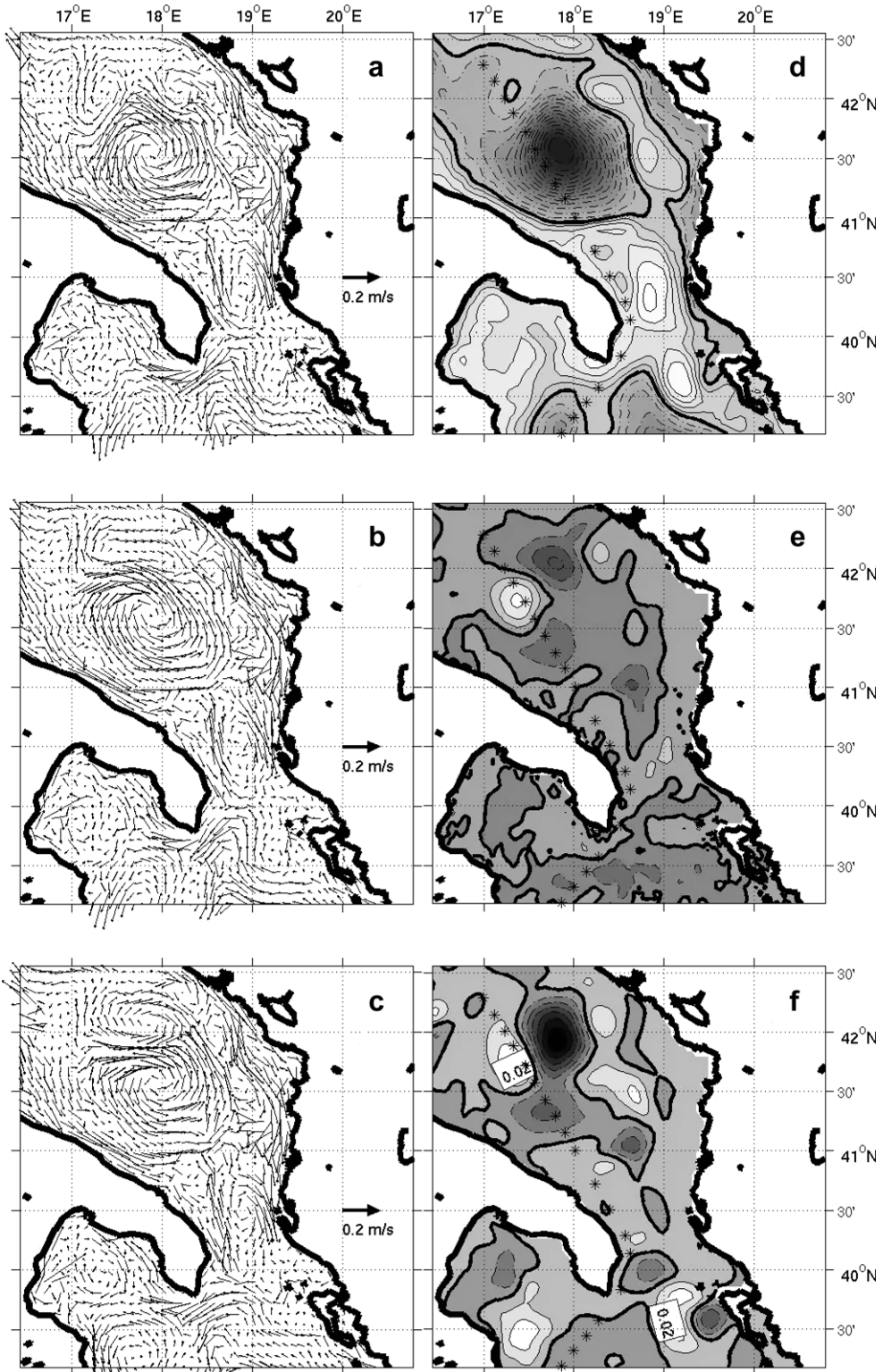


Fig. 8. Same as Fig. 7 but for 2–3 December.

decomposition approach especially between 200 and 400 m. The vertically averaged RP are close to 15% for Exp3R and 8% for Exp2R.

In order to understand better the differences between the three experiments we show the barotropic velocity field and the surface elevation for April and December cruises. These variables have been averaged over the period of the cruises. It has to be pointed out that differences in the ocean’s interior responses could be due to internal intrinsic variability modes, not directly related to information propagating from the boundaries. Analyzing the surface elevation field and the differences between experiments with different lateral boundary conditions (Figs. 7, 8 and 10) we will try to separate the causes of the differences.

In Fig. 7 the simulations corresponding to the April cruise are shown. The barotropic velocity fields for the Exp1R and Exp2R along the XBT tracks have similar patterns, the major differences being in the small structures developing in the Otranto Channel (Fig. 7d) and at the borders of the Southern Adriatic (SAd) cyclonic gyre. This gyre (Fig. 7d) is a permanent feature of the Adriatic circulation (Artegiani et al., 1997a; Artegiani et al., 1997b). In Exp3R the SAd gyre is closer to the Italian coast with respect to the other two experiments. The different spatial configuration of the circulation close to the open boundary is emphasized when comparing the surface elevation fields. The model reacts to Exp2R and Exp3R lateral boundary conditions in a different way. In both simulations the cyclonic character of the circulation is slightly amplified close to the open boundary, but the scale selective approach produces a more coherent pattern extending from the boundary to the interior of the model domain.

In Fig. 8 the results for the December period are shown. During December differences are evident in the position and intensity of the SAd gyre. In this period, and in all experiments, small anticyclonic structures encircle the SAd gyre on its north-eastern side. Their number and intensity, however, are strongly affected by the boundary conditions. In Exp1R two anticyclonic gyres are present on the eastern side of the SAd. In Exp2R the same two structures are almost connected forming a single large feature, while in Exp3R the

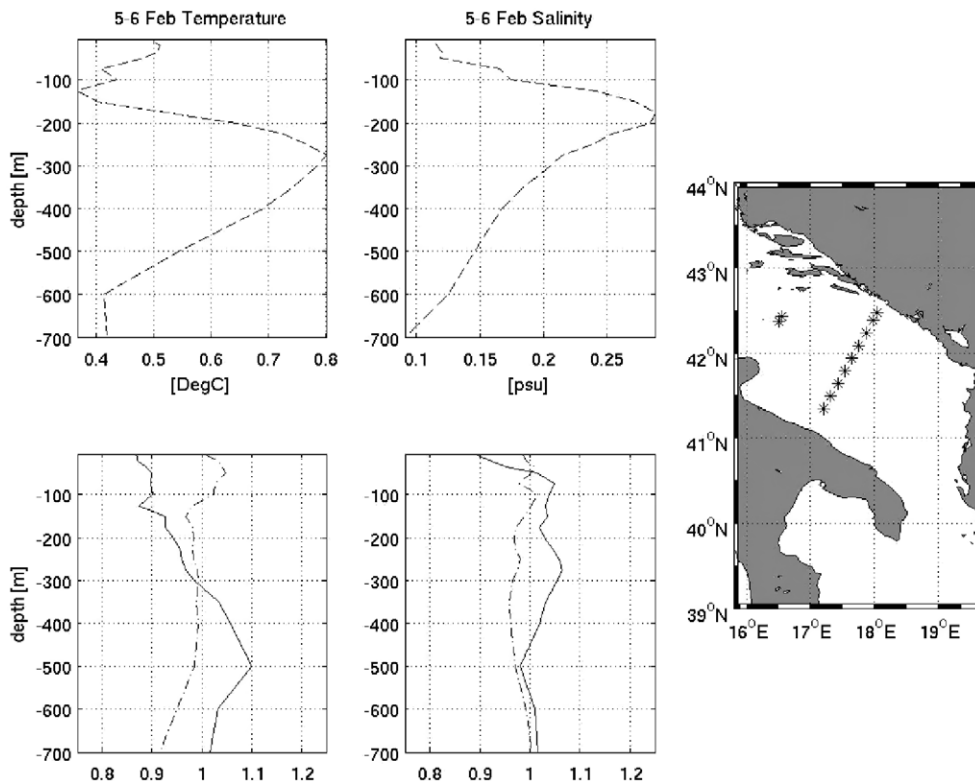


Fig. 9. Vertical profiles of Temperature and Salinity RMS errors, Relative Performance-RP index and CTD sampling positions for 5–6 February 2001. The first row shows the vertical profiles of RMS temperature and salinity error for the reference experiment (Exp1R). In the second row the RP of Exp2R (dashed line) and Exp3R (solid line) are shown. The right plot shows the position of the CTD casts.

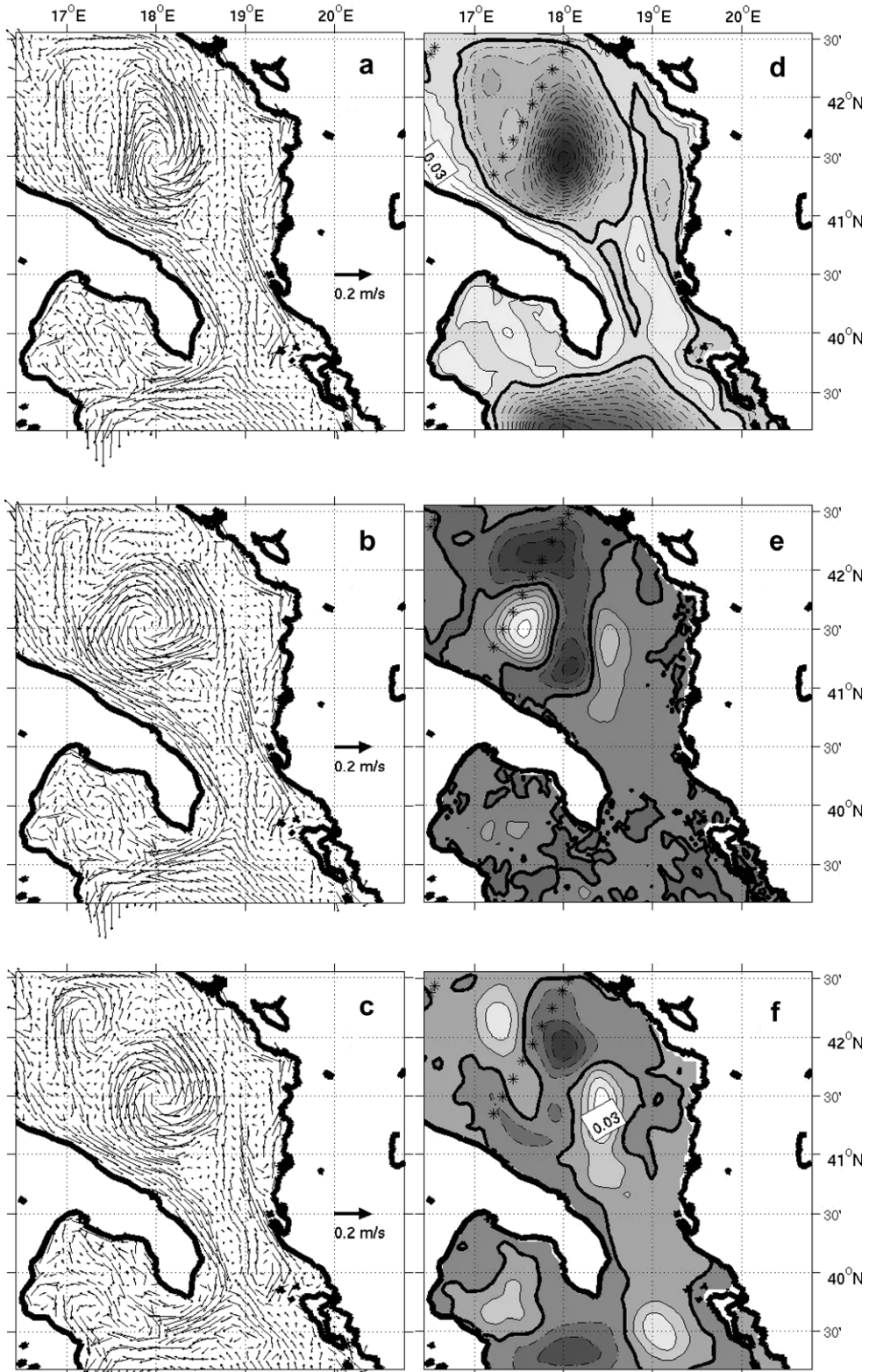


Fig. 10. Same as Fig. 7 but for 5–6 February.

two anticyclones are smaller. Important differences are evident comparing the Fig. 8 surface elevation fields south of the Otranto Strait. In the surface elevation difference field between Exp1R and Exp2R no clear structures can be found at the lateral boundary while the model response to scale selective boundary conditions results in an amplification of the cyclonic character of the circulation. For this specific period, the differences shown in Fig. 8 do not exhibit clear and coherent patterns, and the small anticyclonic structures encircling the SAd gyre appear to be more the results of model intrinsic internal variability.

In Fig. 9 the temperature and salinity RMS error and RP index vertical profiles of the different experiments for a CTD cruise (5–6 February 2001) are shown together with the corresponding sampling positions. In terms of temperature Exp3R gives better results in the upper layers with respect to the two others experiments, but worse results from 300 to 600 m depth. For salinity Exp3R gives the maximum error between 200 and 300 m. A possible explanation of this salinity error can be given in terms of the limited capability to reproduce levantine intermediate water (LIW) intrusion in the Adriatic Sea by the coarse resolution model solution. The LIW is a large scale feature and its correct representation in the regional model totally depends on the nesting model solution. Large errors in the LIW salinity values have been found analyzing the nesting model solution in the same section (not shown). Therefore a better representation of the water masses exchanges through the lateral open boundary conditions can cause a deterioration of the solution within the regional model domain.

The barotropic circulation on 5–6 February (Fig. 10) for Exp1R is characterized by a SAd gyre containing two cyclonic sub-gyres, one stronger south of the CTD section and the second smaller on its northern side. In Exp2R the SAd larger sub-gyre mainly extends in the W–E direction, it is enhanced at the surface and without

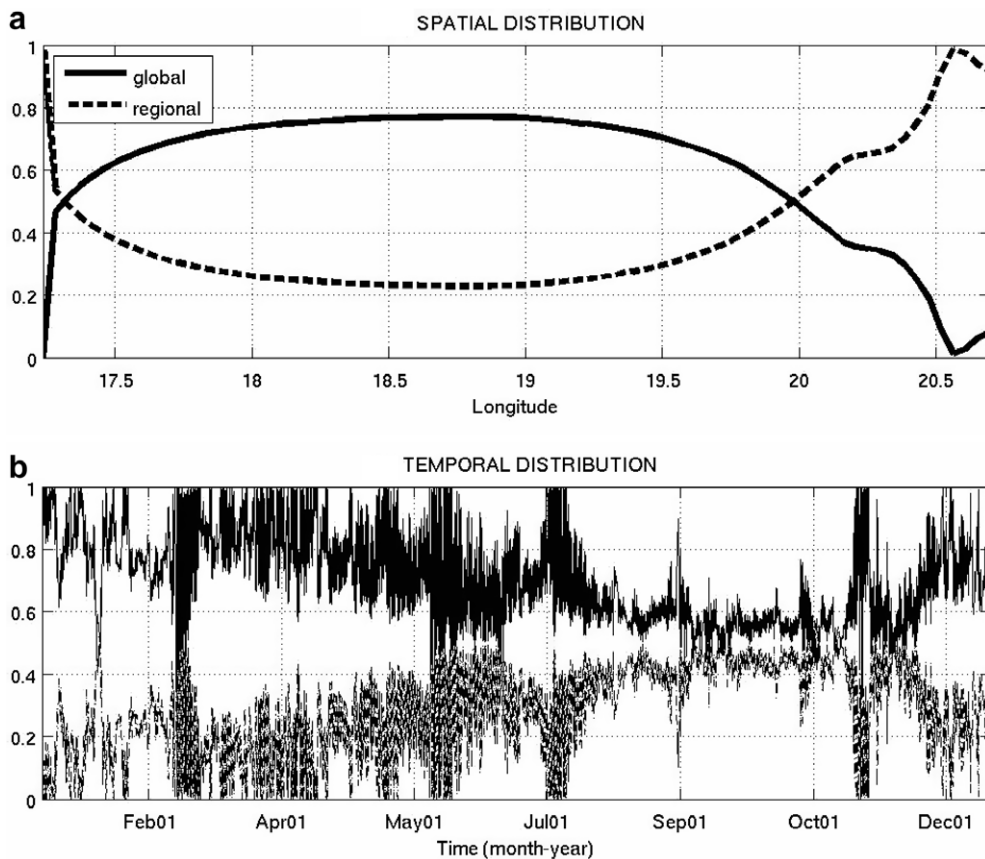


Fig. 11. (a) Time average of the global and regional component weights of the surface elevation along the open boundary line. (b) Time series of the global and regional surface elevation field weights. In both the panels, the solid line indicates the weight of the global field, the dashed line indicate the weight of the regional component.

the smaller cyclonic sub-gyre on its northern tip. The surface elevation fields near the boundaries show evidence that in Exp2R the numerical noise is largest. The SAd gyre reproduced by Exp3R is the most symmetric. Fig. 10(f) clearly indicates that the differences in the reproduced interior structures are driven by lateral boundary condition dynamic, since a clear and continuous flow extends from the southern limit of the model domain to the northern inner part.

In Fig. 11 the time (a) and spatial (b) averaged weights (over 2001) of the global and regional components of the surface elevation are shown. The relative weight is defined as $|\frac{u_g}{u_r}|$ for the global and $|\frac{u_r}{u_g}|$ for the regional component. The global component is dominant in the centre of the open boundary where the bathymetry is deeper, and represents almost 80% of the total field (Fig. 11a). Close to the coasts the weight of the regional component increases. Near the Italian coast (left side of the subplot A), where the topography has steeper gradients, the influence of the regional part decreases with a faster rate going offshore than on the other side of the boundary line. The regional component is dominant in the eastern part of the boundary. Beyond what discussed in Section 5.1 for the idealized case, a possible explanation for this spatial distribution of regional and global surface elevation components is related to the coarse resolution of the nesting model that makes the whole coastal area a region of viscous boundary layer where the velocity is almost zero. Thus the regional solution emerges as the most important one.

In Fig. 11b the time series of the free surface components relative weights averaged over all the boundary line are shown. The sampling interval is about 10 min. The plot clearly indicates that high frequency oscillations are modulated by a large seasonal cycle.

During the winter and autumn seasons the global component dominates the boundary regime. On the other hand, during spring and summer the regional and global components have similar weights. It is probably a consequence of the mesoscale dynamics in this region that rapidly develop during the calm wind regimes. The larger eddy structure of the summer circulation has been depicted by many authors in the Mediterranean and Adriatic Sea (Artegiani et al., 1997a; Ayoub et al., 1998; Millot, 1991). The amplitudes of the high frequency oscillations and of the seasonal signal are similar. Moreover, it is interesting to note that the large high frequency oscillations appearing throughout the year have similar frequency to the atmospheric forcing (approximately 6 h).

6. Summary and conclusions

The most commonly used lateral open boundary conditions were reviewed and a formal derivation of the barotropic velocity lateral boundary condition is presented in this paper. The result is a generalized Flather boundary condition Eq. (14) and the possibility to apply a scale selective approach to the lateral boundary conditions.

We derived the Flather (1976) boundary condition in order to use the derivation for the development of a new scale decomposition method. One of the main conceptual problems in the Flather (1976) lateral boundary condition are the simplifications made in its derivation. However, our new formulation of Flather (1976) done in (14) relaxes these simplifications and use a more complete formulation of the lateral boundary conditions for barotropic normal velocities. After decomposing the nested model fields in ‘global’ and ‘regional’ components (16), we have derived two new general lateral boundary conditions, (23) and (26) for the barotropic velocity components.

Idealized and realistic numerical experiments have been carried out in order to study the impact of the scale selective lateral boundary conditions.

In the idealized experiments results are easier to understand and show significant improvements in the model solution related to the application of the scale selective approach to the lateral boundary conditions problem. Due to the model configuration and the present implementation of the new method, major improvements are actually confined in the shallow water areas.

A system composed by a coarse model with rigid lid, covering the entire Mediterranean Sea, and a fine resolution free surface model, reproducing the Adriatic Sea, has been used to evaluate the performance of different boundary conditions in a realistic framework. Three test cases in the realistic framework have been presented and the results discussed. The simple condition for barotropic and total velocity with an advection scheme for the tracers (Exp1R), the 2D version of the radiation condition as proposed by Marchesiello et al.

(2001) for all the model variables (Exp2R), and the scale decomposition approach for the barotropic velocity, the imposition of the total velocity and an advection scheme for the tracers (Exp3R).

The boundary condition choice affects the model solution in the interior domain in terms of position and intensity of the circulation structures. These differences are amplified during specific periods. The Exp2R (2D radiation) solution appears affected by numerical noise in the area close to the open boundary even though this numerical disturbance does not seem to affect the interior solutions. Especially during April and December the scale decomposition approach gives better results in terms of RMS error between model results and observations. As a final note, we would like to point out that, at the present time, we are still far from a general solution for the lateral boundary condition problem. Moreover we believe that the scale selective approach can represent an important step in the research of the general solution.

Future work will be directed toward the testing of the process-scale decomposition for other variables and types of nested models.

Acknowledgement

We thank two anonymous reviewers for very interesting comments that were included in the manuscript. The authors also would like to thank Dr. P.F.J. Lermusiaux for discussion and suggestions that improved and clarified this paper. This work was partially supported by the MERSEA project (EU project FP6 SIP3-CT-2003-502885) and the ADRICOSM Pilot Project, funded by the Italian Ministry of Environment.

References

- Artegiani, A., Bregant, D., Paschini, E., Pinardi, N., Raicich, F., Russo, A., 1997a. The Adriatic Sea general circulation Part I: Air sea interaction and water mass structure. *J. Phys. Oceanogr.* 27, 1492–1514a.
- Artegiani, A., Bregant, D., Paschini, E., Pinardi, N., Raicich, F., Russo, A., 1997b. The Adriatic Sea general circulation Part II: Baroclinic circulation structure. *J. Phys. Oceanogr.* 27, 1515b–1532b.
- Ayoub, N., Le Traon, P.Y., De Mey, P., 1998. A description of the Mediterranean surface circulation from combined ERS-1 and TOPEX/POSEIDON altimetric data. *J. Mar. Sys.* 18 (1–3), 3–40.
- Bennett, A.F., Kloeden, P.E., 1978. Boundary conditions for limited-area forecasts. *J. Atmos. Sci.* 35, 990–996.
- Blayo, E., Debreu, L., 2005. Revisiting open boundary conditions from the point of view of characteristic variables. *Ocean Modell.* 9, 231–252.
- Blumberg, A.F., Mellor, G.L., 1987. A description of a three-dimensional coastal ocean circulation model. In: Heaps, N.S. (Ed.), *Three-dimensional coastal ocean models*. American Geophysical Union, Washington, DC, p. 208.
- Chapman, D.C., 1985. Numerical treatment of cross-shelf open boundaries in a barotropic coastal ocean model. *J. Phys. Oceanogr.* 15, 1060–1075.
- Demirov, E., Pinardi, N., 2002. Simulation of the Mediterranean Sea circulation from 1979 to 1993: Part I. The interannual variability. *J. Mar. Syst.*, 23–50.
- Flather, R.A., 1976. A tidal model of the northwest European continental shelf. *Memories de la Societe Royale des Sciences de Liege* 6 (10), 141–164.
- Lermusiaux, P.F.J., 2007. Adaptive modeling, adaptive data assimilation and adaptive sampling. *Physica D*, doi:10.1016/j.physd.2007.02.014.
- Marchesiello, P., McWilliams, J.C., Shchepetkin, A., 2001. Open boundary conditions for long term integration of regional oceanic models. *Ocean Modell.* 3, 1–20.
- Mellor, G.L., Yamada, T., 1982. Development of a turbulence closure submodel for geophysical fluid problems. *Rev. Geophys. Space Phys.* 20, 851–875.
- Millot, C., 1991. Mesoscale and seasonal variabilities of the circulation in the western Mediterranean. *Dynam. Atmos. Oceans* 15, 179–214.
- Miyakoda, K., Rosati, A., 1977. One-way nested grid models: The interface conditions and the numerical accuracy. *Monthly Weather Rev.* 105 (9), 1092–1107.
- Nihoul, J.C.J., Djenidi, S., 1998. Coupled physical, chemical and biological models. In: Brink, K.H., Robinson, A.R. (Eds.), *In: The Sea: The Global Coastal Ocean I" Processes and Methods*, Vol.10. John Wiley and Sons, New York, NY.
- Oddo, P., Pinardi, N., Zavatarelli, M., 2005. A numerical study of the interannual variability of the Adriatic Sea (2000–2002). *Sci. Total Environ.* 353 (1–3), 39–56.
- Oddo, P., Pinardi, N., Zavatarelli, M., Coluccelli, A., 2006. The Adriatic Basin Forecasting System. *Acta Adriatica* 47 (Suppl.), 169–184.
- Orlanski, I., 1976. A simple boundary condition for unbounded hyperbolic flows. *J. Comput. Phys.* 21, 251–269.
- Oliger, J., Sundstrom, A., 1978. Theoretical and practical aspects of some initial boundary value problems in fluid mechanics. *SIAM J. Appl. Math.* 35, 419–446.

- Palma, E.D., Matano, R.P., 1998. On the implementation of passive open boundary conditions for a general circulation model: the barotropic mode. *J. Geophys. Res.* 103, 1319–1341.
- Palma, E.D., Matano, R.P., 2000. On the implementation of open boundary conditions for a general circulation model: the three-dimensional case. *J. Geophys. Res.* 105, 8605–8628.
- Perkins, A.L., Smedstad, L.E., 1998. Scale-Related Aspects of Nested Finite Difference Ocean Models. *Theor. Comp. Fluid Dyn.* 10, 311–322.
- Perkins, A.L., Smedstad, L.F., Blake, D.W., Heburn, G.W., Wallcraft, A.J., 1997. A new nested boundary condition for a primitive equation ocean model. *J. Geophys. Res.* 102 (C2), 3483–3500.
- Pinardi, N., Rosati, A., Pacanowski, R.C., 1995. The sea surface pressure formulation of rigid lid models implications for altimetric data assimilation studies. *J. Mar. Sys.* 6, 109–119.
- Pinardi, N., Allen, I., Demirov, E., De Mey, P., Korres, G., Lascaratos, A., Traon, P.Y., Maillard, C., Manzella, G., Tziavos, C., 2003. The Mediterranean ocean forecasting system: first phase of implementation (1998–2001). *Ann. Geophys.* 21, 3–20.
- Raymond, W.H., Kuo, H.L., 1984. A radiation boundary condition for multidimensional flows. *Q. J. Roy. Meteor. Soc.* 110, 535–551.
- Smagorinsky, J., 1993. Some historical remarks on the use of nonlinear viscosities. In: Galperin, B., Orszag, S.A. (Eds.), *Large eddy simulations of complex engineering and geophysical flows*. Cambridge University Press, New York.
- Spall, M.A., Robinson, A.R., 1989. A new open ocean, hybrid coordinate primitive equations model. *Math. Comput. Simulat.* 31, 241–269.
- Sommerfield, A., 1949. In: *Partial differential equations Lecture Notes on Theoretical Physics*, Vol. 6. Academic Press, San Diego, CA.
- Temam, R., Tribbia, J., 2003. Open Boundary Conditions for the Primitive and Boussinesq Equations. *J. Atmos. Sci.* 60 (21), 2647–2660.
- Zavatarelli, M., Pinardi, N., Kourafalou, V.H., Maggiore, A., 2002. Diagnostic and prognostic model studies of the Adriatic Sea circulation. Seasonal variability. *J. Geophys. Res.* 107 (C1), art 3004.
- Zavatarelli, M., Pinardi, N., 2003. The Adriatic Sea modelling system: a nested approach. *Ann. Geophys.* 21, 345–364.